LEGIBILITY NOTICE

A major purpose of the Technical Information Center is to provide the broadest dissemination possible of information contained in DOE's Research and Development Reports to business, industry, the academic community, and federal, state and local governments.

Although a small portion of this report is not reproducible, it is being made available to expedite the availability of information on the research discussed herein.

LA-UR -1184

LA-UR--88-1184

DE88 009144

TITLE SHOCK COMPACTION OF RAPIDLY SOLIDIFIED NICKEL BASED Mo-Al-W ALLOY POWDERS WITH PRESSURE UP TO 1.2 MBAR

AUTHOR(S) Karl Paul Staudhammer, MST-7

SUBMITTED TO HERAPS'88 International Seminar on High Energy Working of Rapidly Solidified Materials, Invited presentation
Novosibirsk, USSR
October 10-14, 1988

DISCLAIMER

MASTER

Los Alamos National Laboratory
Los Alamos, New Mexico 87545

SHOCK COMPACTION OF RAPIDLY SOLIDIFIED NICKEL BASED Mo-Al-W ALLOY POWDERS WITH PRESSURES UP TO 1.2 MBAR

K. P. STAUDHAMMER
Los Alamos National Laboratory
Materials Science & Technology Division
Los Alamos, New Mexico 87545

Alloys produced by rapid quenching from the melt have been shown to exhibit metallurgical characteristics not obtainable by conventional casting methods. Such features include refined grain size, extended solid solutions [1,2], metastable phases [3,4], and metallic glasses [5-7]. Super alloys are among the best examples of grain growth control in commercial practice today. The alloys of interest are based on nickel with alloying additions of aluminum to form the strengthening gamma prime phase, refractory metals such as Mo and W, to provide solid solution strengthening and various interstitial and other minor elements to provide grain boundary strengthening, oxidation, corrosion resistance, etc.

The alloy described in this paper is a high strength nickel alloy containing 10 wt% Mo, 6.8 wt% Al, and 6 wt% W. It cannot be easily prepared by conventional casting methods without gross segregation occurring in the form of massive dendrites. Gas atomization to form fine powders reduces the dendrite size and therefore, the segregation. The spacing of the secondary dendrite arm has been used to estimate the cooling rate of this powder. A cooling rate in the range of 10^4 to 10^5 K/s [8,9] was obtained for particles smaller than 100μm in diameter. These powders are shown in fig. 1.

The experimental investigation of shock compaction is based in part on the mach stem lens formation work by C. E. Morris, R. G. McQueen, and S. P. Marsh [10]. One of the fortuitous aspects of the cylindrical explosion design is its suitability as a screening tool with its very high success rate of recovery. The designs allow the experimenter to observe in one shot a wide variety of pressure and strain

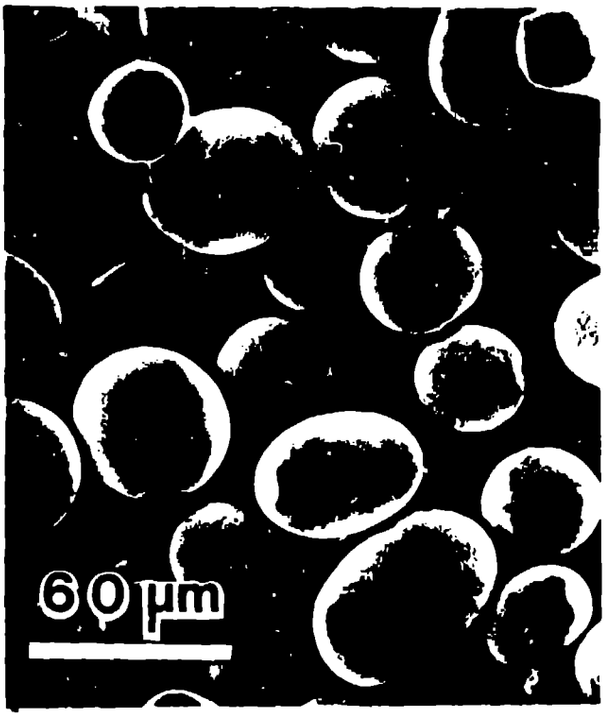

Fig. 1. Scanning electron micrograph of as received RSR Nickel-10Mo-6.8Al-6W alloy powder.

variables necessary to characterize optimum compaction and or consolidation as a function of initial powder densities. Previous investigations [11] have shown the effectiveness of this technique using 304 stainless steel powders [12]. The unique microstructure of the Rapid Solidification Rate (RSR) powder was chosen to help characterize and deliniate the effects of the shock conditions. It should be emphasized that the powder was selected to help in the modeling of the formation of the mach stem zone (over compacted) and that this technique is not particularly used or recommended to compact RSR powder.

The shock loading assembly is shown in fig. 2. This design and its modified versions are discussed in several papers [10, 13-15]. The shock assembly consists of a tube welded in vacuum containing the sample of interest inserted into the central axis of a 0.95cm diameter right cylinder 6.7cm long which was set on a 5.10cm pedestal of the same diameter. The test sample was surrounded by composition C-4 explosive (having a density of 1.59 g/cc and a detonation velocity of 8.04 mm/µs) and then encased in a steel recovery assembly. Initiation of the explosive occurs around the outer edge of the top of the sample recovery cylinder. The detona-

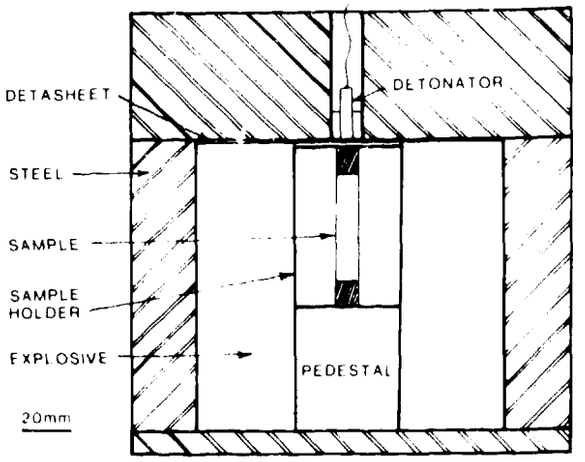

Fig. 2. Schematic of shock loading design.

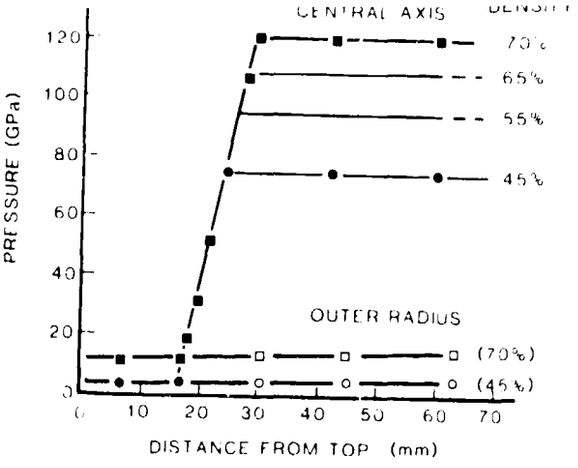

Fig. 3. Hydrocode calculations of achieved pressure versus axial length as a function of initial density.

tion wave moves down along the outer edge of the cylinder and out into the explosive. The sweeping shock wave generated by the explosive converges at the center of the cylinder which creates a high pressure region called the Mach stem. The terminal shock velocity achieved is the detonation velocity of the explosive and this determines the maximum pressure which can be attained for any given initial density of powder compact. During the time of formation of the Mach stem, the powder in the central tube experiences increasing shock pressures with increasing distance down the tube length. At the top the pressure is approximately 12 GPa and increases to 120 GPa at the bottom of the holder for an initial density of 70%.

As the powder density changes, the magnitude of the pressure "seen" by the powder also changes. These densities are shown in fig. 3. Hydrocode computer calculations were employed to determine shock pressures experienced by the powder. These calculations employed a two-dimensional Eularian code which has the ability to incorporate multi-materials, material strengths, equation-of-state, and programmed burn rate for the high explosives. A radial pressure profile at an axial length of 42mm is shown in Figure 4 for a powder having an initial density of 68%. The RSR powder experiences a pressure from 58 GPa to a maximum of 118 GPa at the central axis.

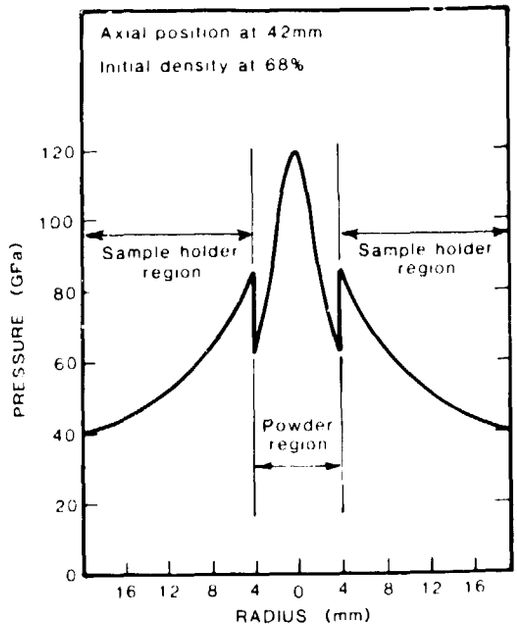

Fig. 4. Calculated pressure versus radial position in the powder sample.

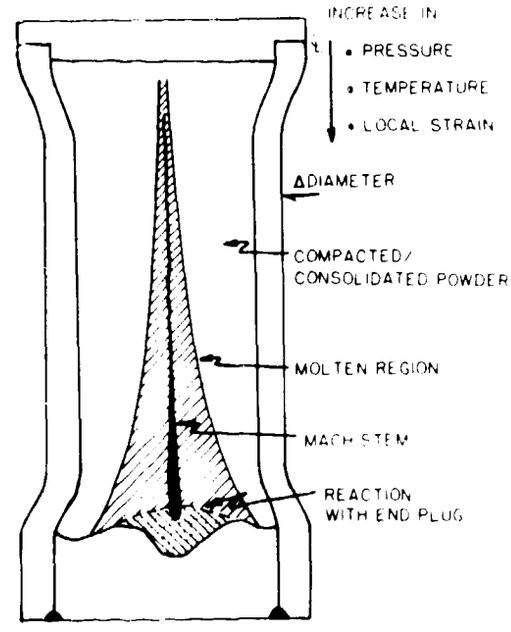

Fig. 5. Cross section schematic of cylindrical RSR sample showing postshocked characteristics.

RESULTS

A cross sectional schematic of a post shocked RSR specimen holder is shown in fig. 5 Of the initial densities investigated (53%, 58%, and 68%) all had similar characteristics to that shown in fig. 5, only variations in magnitude were observed. For example, for lower initial density greater melting and greater decrease in diameter were noted as compared to the higher initial density samples. In the consolidation of these RSR powders the region of interest is outside the central cross hatched region in Figure 5. The further one moves radially out from any given axial length position, the less consolidation is observed and essentially only compaction at the extreme edges of the holder. This observation is illustrated in fig. 6 for 4 axial length positions (the sample holder was cut at these length positions). Each axial length position has a maximum pressure that the RSR powder had experienced at its central axis (left vertical axis of fig. 6). With an increase in radial distance, these pressures drop off, and reflect the same profile as shown in the central portion of fig. 4. Observations of post shocked samples sectioned at axial lengths of 12.5, 19, 24, 28, and 42mm revealed the melt

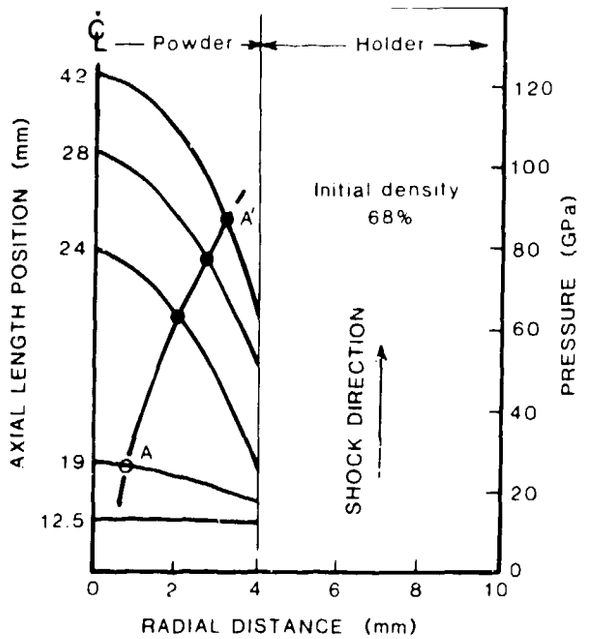

Fig. 6. Pressure versus radial distance (from center line ℄) for selected axial length positions of 12.5, 19, 24, 28, and 42mm in a RSR powder sample having an initial density of 68%. The 42mm axial length corresponds to the right half of the powder region in Figure 4.

zone to follow line A-A' on fig. 6. Regions to the left of line A-A' in axial and radial space all contained pressure-temperature conditions which resulted in total melting of the RSR powders. Below line A-A' regions of consolidation and compaction were observed. It should be noted that this figure only illustrates the above mentioned regions for 68% initial density. As the initial density changes (over some limited range, the profile (shape) of the A-A' curve will change along with the concomitant pressure achieved. In so doing, several samples with varying initial densities were prepared and shocked under the same conditions. Observations of melt, consolidation and compaction were made, similar to that shown in fig. 6. The results of all of these observations are shown in fig. 7. Instead of plotting axial length position and radial distance, pertinent primarily to the test technique used here, fig. 7 shows the compaction, consolidation, and melting regimes achieved at any given pressure for specific packing densities of the RSR powder. The initial density range varied from 53 to 68%.

The increase in the melt zone radius with increased travel of the shock wave is not surprising in light of the increase in pressure and a change from primarily surface

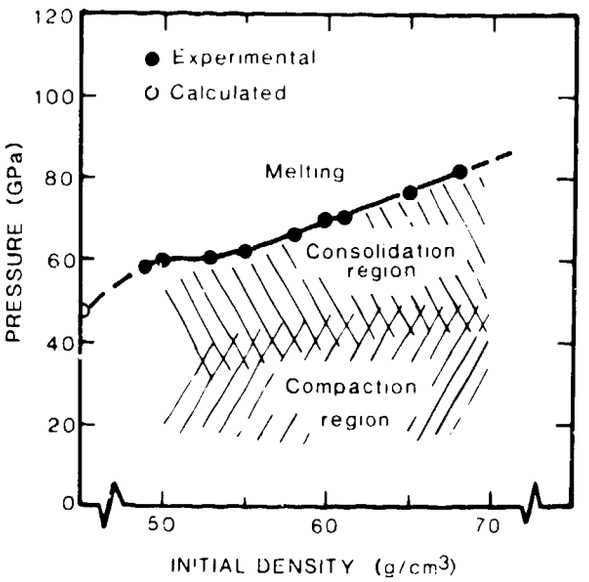

Fig. 7. Pressure versus initial density of the RSR powder. The shaded areas indicate regions of compaction and consolidation. Melting results for pressures which are above the curve.

deformation of particles at low pressures, to more massive non-homogeneous particle deformation at the higher pressures. This is indicative of an increasing entropic temperature as well as adiabatic heating resulting in a large melt zone. This melt zone is more prominent at the 53% than at the 68% initial density, and is due to the greater local particle strain for the lower density as described in [16]. The mach stem zone (neglecting end effects) as shown in fig. 5 does not exceed 0.8mm radius along the central axis and is consistent with the mach stem region calculated in the hydrocode. The melt zone, however, is not accounted for in the hydrocode calculations and does represent an area for further modeling work.

The region indicated in fig. 7 is illustrated in fig. 8. Figure 8a is an SEM micrograph of compacted RSR powder at 12 GPa having an initial density of 68%. Compaction is evident from the morphology change of the powder particles, as well as a lack of interparticle bonding. No interparticle melting was observed at this pressure. Figure 8b is an optical micrograph of a cross section showing very good particle consolidation at 64 GPa.

In this pressure regime, no interparticle voids were observed and near theoretical densities are obtained. Figure 8c is an optical micrograph at the transition between con-

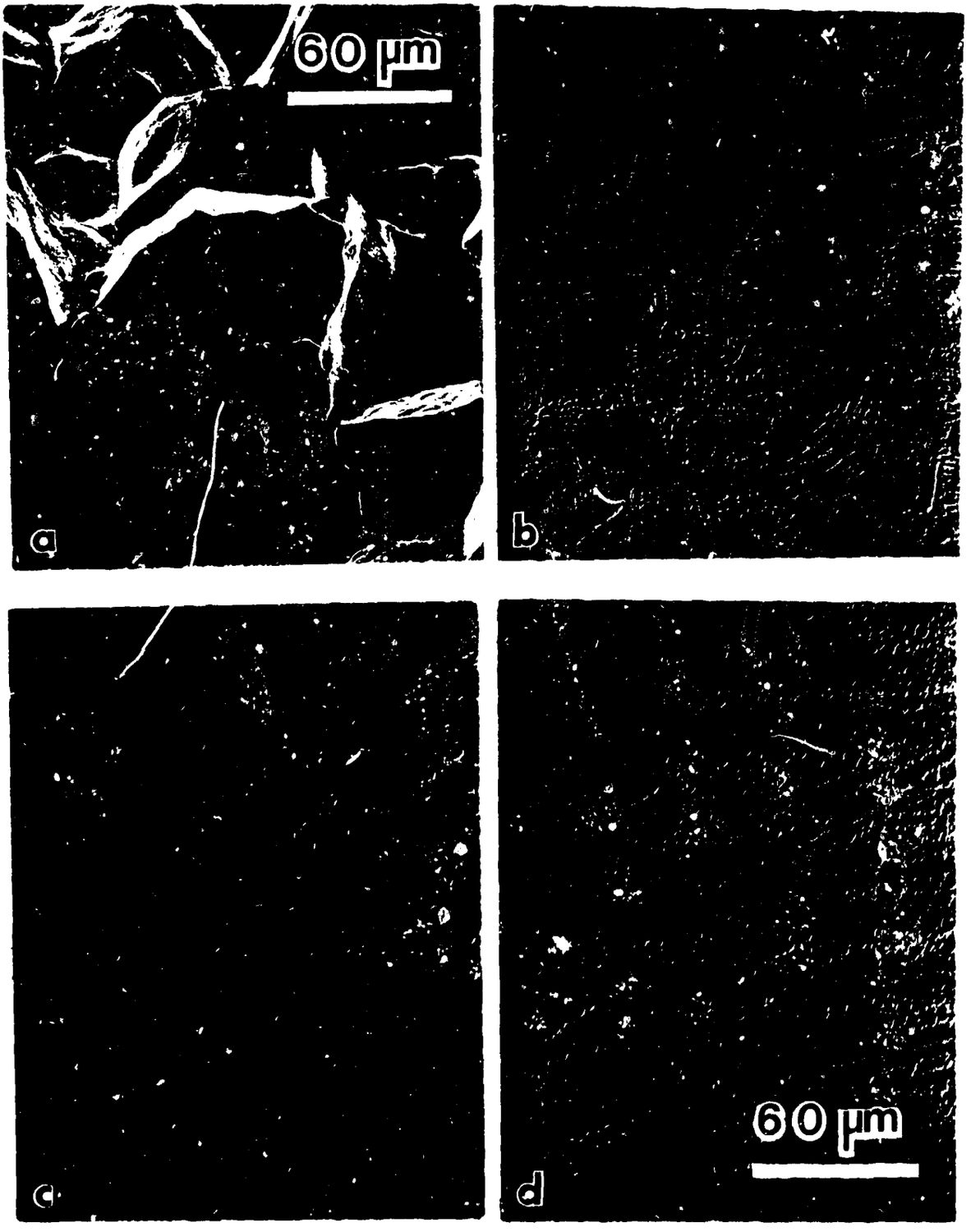

Fig. 8. Micrographs of indicated regions for a RSR sample with an initial density of 68%. a) SEM of undercompacted region at 12 GPa, b) Optical micrograph of a consolidated region at 64 GPa, c) Optical micrograph of transition region between consolidation and melting pressure at 82 GPa, and d) Melt region at 100 GPa.

... melting of the RSR powder at a pressure of 82 GPa. The region on the right is consolidated powder while that on the left has been melted. The increase in dendrite spacing of the melt zone shown in fig. 8D which was shocked at 100 GPa is evident. For this density of packing, pressures above 82 GPa are obviously in excess of that required to consolidate. Similar conditions exist for the lower initial density powders with a concomitant decrease in pressure, as indicated in fig. 7. The transition region shown in fig. 8c has a 40μm thick region of recrystallized grains similar to what is observed in the heat effected zone (HAZ) of a weld. These recrystallized grains averaged from 7μm adjacent to the melt zone down to 2μm adjacent to the consolidated particles. Due to the large variation of dendrite size in the melt region as compared to the dendrite size in the as received RSR powder one is able to correlate the maximum pressure for consolidation as a function of initial density.

SUMMARY

Use of the radial implosion design as described here has allowed for the determination of optimum pressures required for consolidation of RSR Ni-10Mo-6.8Al-6W alloy powders as a function of initial packing density. These sets of experiments are in line with previous work on other shock consolidated powders showed that an increase of initial density decreased the melt zone, and only required a slight increase in the pressure to consolidate.

ACKNOWLEDGEMENTS

The author wishes to thank S. P. Marsh for the hydrocode calculations, A. J. Gray for the metallography, and N. E. Elliott for the SEM work.

REFERENCES

1. B. C. Giessen in: Development in the Structural Chemistry of Alloy Phases, B. C. Giessen, ed. (Plenum, New York 1979) pp. 227-281.
2. H. Jones and C. Suryanarayana, J. Mat. Sci. 8, 705 (1973).
3. P. Ramachandrarso, et al., Phil. Mag. 25, 961 (1972).
4. R. W. Cahn, et al., Mat. Sci. Eng. 23, 83 (1976).

5. D. E. Polk and B. C. Giessen in: Metallic Glasses (ASM, Metals Park, 1978), pp. 1-35.
6. R. W. Cahn, Contemp. Phys. 21, 43 (1980).
7. C. Suryanarayana, Sci. Rep. RITU A-28, 143 (1980).
8. R. H. Van Stone, F. J. Rizzo, and J. F. Radavich in: Rapid Solidification Processing Principles and Technologies II, R. Mehrabian, B. H. Kear, and M. Cohen, eds. (Claitor's Publishing Division, Baton Rouge, 1980), pp. 260-272.
9. V. Anand, A. J. Kaufrian, and N. J. Grant, Ibid, pp. 273-286.
10. C. E. Morris, R. G. McQueen, and S. P. Marsh, Shock Waves in Condensed Matter - 1983, Proceedings of the American Physical Society Topical Conference, Santa Fe, New Mexico, 1983, North Holland, pp. 207-10, 1984.
11. K. A. Johnson and K. P. Staudhammer, "EXPLOMET 85," L. E. Murr, K. P. Staudhammer, and M. A. Meyers, ed., Marcel Dekker, March 1986, pp. 525-42.
12. K. P. Staudhammer and K. A. Johnson, Ibid, pp. 149-166.
13. K. A. Johnson, L. E. Murr, and K. P. Staudhammer, Acta Metall., Vol. 33, No. 4, pp. 677-84, 1985.
14. K. P. Staudhammer, K. A. Johnson, and B. Olinger, Shock Waves in Condensed Matter, J. R. Asay, R. A. Graham, G. K. Straub (eds.), (Elsevier Sci. Pub., 1983), 419-422.
15. K. P. Staudhammer and K. A. Johnson, International Conference on Impact Loading and Dynamic Behavior of Materials, Bremen, West Germany, May 18-21, 1987, in print.
16. K. P. Staudhammer and L. E. Murr, in Industrial Applications of Shock Waves, Chapter 7, edited by L. E. Murr, to be published.